

An energy conserving finite-difference model of Maxwell's equations for soliton propagation

H.Bachiri, L.Gilles, and L.Vázquez

Departamento de Matemática Aplicada, Escuela Superior de Informática,

Universidad Complutense, E-28040 Madrid, Spain.

E-mail : lucgil@eucmax.sim.ucm.es

A.M.S. Classification : 65C20, 78A40.

Abstract

We present an energy conserving leap-frog finite-difference scheme for the nonlinear Maxwell's equations investigated by Hile and Kath [C.V.HILE and W.L.KATH, *J.Opt.Soc.Am.B* **13**, 1135 (1996)]. The model describes one-dimensional scalar optical soliton propagation in polarization preserving nonlinear dispersive media. The existence of a discrete analog of the underlying continuous energy conservation law plays a central role in the global accuracy of the scheme and a proof of its generalized nonlinear stability using energy methods is given. Numerical simulations of initial fundamental, second and third-order hyperbolic secant soliton pulses of fixed spatial full width at half peak intensity containing as few as 4 and 8 optical carrier wavelengths, confirm the stability, accuracy and efficiency of the algorithm. The effect of a retarded nonlinear response time of the media modeling Raman scattering is under current investigation in this context.

1 Introduction

Computational modeling of Maxwell's equations using finite-difference time domain methods has been shown simple in concepts and execution, allowing accurate predictions for a wide range of optical phenomena [1], in particular for optical soliton propagation [2]. One of the fundamental advantages in solving directly the nonlinear Maxwell's equations instead of scalar generalized nonlinear Schrödinger equations for the slowly varying envelope of the optical pulses is that scattering, diffraction and short pulse effects are retained in the former approach [3] since all the electromagnetic components without eliminating the carrier are taken into account.

In this paper we solve numerically Maxwell's equations describing scalar one-dimensional optical soliton propagation in nonlinear media of arbitrary dispersion proposed in Ref.[4]. We implement an efficient leap-frog finite-difference time domain numerical method. The fundamental difference with the leap-frog method used in Ref.[4] is that our scheme has a discrete analog of the underlying continuous energy conservation law, which lies at the basis of its global accuracy and stability. We give an explicit proof of its generalized nonlinear stability using known results on energy methods [5, 6, 7].

The paper is organized as follows. In Section 2 we present the model and derive the exact energy conservation law. Section 3 deals with the conservative finite-difference scheme and its main properties. The discrete energy conservation law is established and generalized stability is analyzed in Section 4. Finally, we give numerical results in Section 5 for the propagation of fundamental, second and third-order hyperbolic secant solitons of fixed full width at half peak intensity (FWHM) containing as few as 4 and 8 optical carrier wavelengths. Appendix A is devoted to a short linear stability analysis and Appendix B to the numerical dispersion relation. We show how the speed of a moving coordinate system can be adjusted in order to reduce the numerical phase velocity error of the pulse to one part in 10^5 , which is small compared to the physical dispersion being modeled.

2 The Model System

Propagation of light in nonlinear dispersive optical media is governed by Maxwell's equations expressed in terms of \mathbf{E} and \mathbf{H} , the electric and magnetic fields respectively, (considered as primary field quantities) and \mathbf{D} and \mathbf{B} , the derived electric and magnetic flux densities,

$$\begin{aligned}\nabla \times \mathbf{E} &= -\partial \mathbf{B} / \partial t, \\ \nabla \cdot \mathbf{B} &= 0, \\ \nabla \times \mathbf{H} &= \partial \mathbf{D} / \partial t, \\ \nabla \cdot \mathbf{D} &= 0.\end{aligned}\tag{1}$$

We choose the constitutive relations (depending on the nature of the media considered) of the form

$$\begin{aligned}\mathbf{B} &= \mu_0 \mathbf{H}, \\ \mathbf{D} &= \epsilon_0 [\mathbf{E} + \mathbf{\Phi} + \mathbf{\Phi}^{NL}],\end{aligned}\tag{2}$$

where μ_0 and ϵ_0 are the free-space permeability and permittivity, and $\mathbf{\Phi}$, $\mathbf{\Phi}^{NL}$ are the induced linear and nonlinear electric polarizations, which are related to the electric field through the following relation :

$$\begin{aligned}\mathbf{\Phi} &= \int_{-\infty}^t \chi^{(1)}(t-t_1) \mathbf{E}(t_1) dt_1, \\ \chi^{(1)}(t) &= 0 \quad t < 0, \\ \mathbf{\Phi}^{NL} &= \int_{-\infty}^t \chi^{(3)}(t-t_1, t-t_2, t-t_3) : \prod_{i=1}^3 \mathbf{E}(t_i) dt_i.\end{aligned}\tag{3}$$

Note that in deriving (3) we have assumed centro-symmetric media (like silica glasses), i.e. we have ignored second-order nonlinear effects (second harmonic generation). We further sim-

plify Maxwell's equations by considering isotropic and homogeneous media, allowing a one-dimensional (chosen to coincide with the \mathbf{x} -direction), mono-mode, polarization preserving formulation of the electromagnetic field propagation problem, appropriate to waveguide structures. The time delay of the nonlinear response function $\chi^{(3)}$ will be investigated in a separate publication and is ignored in the present analysis. We assume here that time dependence of the nonlinear susceptibility factorizes in a product of three delta-Dirac distributions $\chi^{(3)}(t_1, t_2, t_3) = a\delta(t_1)\delta(t_2)\delta(t_3)$. We choose for simplicity the case of circularly polarized fields $\mathbf{E} = (0, E_y, E_z)^T$, $\mathbf{H} = (0, H_y, H_z)^T$ with

$$\begin{aligned} E_y(x, t) &= (1/2) q(x, t) \exp[i(k_0 x - \omega_0 t)] + c.c., \\ E_z(x, t) &= (1/2) q(x, t) \exp[i(k_0 x - \omega_0 t - \pi/2)] + c.c., \\ H_y(x, t) &= (1/2) h(x, t) \exp[i(k_0 x - \omega_0 t - \pi/2)] + c.c., \\ H_z(x, t) &= -(1/2) h(x, t) \exp[i(k_0 x - \omega_0 t)] + c.c., \end{aligned} \quad (4)$$

where $q(x, t), h(x, t)$ are complex amplitudes modulating the forward travelling optical carrier. To obtain a *scalar complex* description, we construct the following new fields

$$\begin{aligned} E(x, t) &= (E_y + iE_z) = q(x, t) \exp[i(k_0 x - \omega_0 t)], \\ H(x, t) &= (iH_y - H_z) = h(x, t) \exp[i(k_0 x - \omega_0 t)], \\ D(x, t) &= (D_y + iD_z) = d(x, t) \exp[i(k_0 x - \omega_0 t)]. \end{aligned} \quad (5)$$

Maxwell's equations for the rotated fields are then given by

$$\begin{cases} \mu_0 H_t = E_x, \\ D_t = H_x, \\ D = \epsilon_0 [E + \Phi + \Phi^{NL}], \end{cases} \quad (6)$$

where subscripts refer to derivatives and

$$\begin{aligned} \Phi(x, t) &= \int_0^\infty \chi^{(1)}(t_1) E(x, t - t_1) dt_1, \\ \Phi^{NL}(x, t) &= a E(x, t) |q(x, t)|^2. \end{aligned} \quad (7)$$

Note that if Φ and Φ^{NL} are both zero (vacuum), the particular choice of rotated fields (5) simplify Maxwell's equations to $\mu_0 H_t = E_x$, $\epsilon_0 E_t = H_x$, which are invariant under the substitution $E' = K\mu_0 H$, $H' = K\epsilon_0 E$ (duality property).

To describe chromatic dispersion [3] (accounted for by the linear polarization Φ) we adopt the usual Lorentz model for the refractive index, namely we take $\chi^{(1)}(t)$ of the form

$$\chi^{(1)}(t) = \frac{\beta_1 \omega_1^2}{\nu_0} \exp(-\gamma t) \sin(\nu_0 t) \Theta(t), \quad (8)$$

where $\nu_0 \equiv \sqrt{\omega_1^2 - \gamma^2}$, ω_1 and β_1 are resp. the frequency and strength of the atomic resonance, $\Theta(t)$ is the Heaviside function and γ is a small phenomenological damping constant. The linear refractive index is then written as

$$n_0^2(\omega) = 1 + \hat{\chi}^{(1)}(\omega) = 1 + \frac{\beta_1 \omega_1^2}{\omega_1^2 - 2i\gamma\omega - \omega^2}. \quad (9)$$

We can easily check that the linear polarization satisfies the following differential equation :

$$\Phi_{tt} + 2\gamma\Phi_t + \omega_1^2\Phi - \beta_1\omega_1^2E = 0. \quad (10)$$

Writing $\Phi_t = U$, we then arrive at the following model equations :

$$\begin{cases} H_t = (1/\mu_0)E_x, \\ D_t = H_x, \\ \Phi_t = U, \\ U_t = -2\gamma U - \omega_1^2\Phi + \beta_1\omega_1^2E, \\ D = \epsilon_0 [E + \Phi + a|E|^2E]. \end{cases} \quad (11)$$

We choose the *initial* electric field of the form

$$E(x, t = 0) = E_0\eta_1 \operatorname{sech}(x/x_0) \exp(ik_0x), \quad (12)$$

where $x_0 = ct_0$ is the characteristic length scale of the initial hyperbolic secant pulse profile of peak amplitude E_0 , and is related to the full width at half peak intensity (FWHM) by $\Lambda = 1.76x_0$. We express for convenience all fields in a dimensionless form as follows

$$\begin{aligned} \tilde{H} &= (H/E_0) \sqrt{\mu_0/\epsilon_0}, & \tilde{D} &= D/(\epsilon_0 E_0), & \tilde{\Phi} &= \Phi/E_0, \\ \tilde{U} &= t_0 U/E_0, & \tilde{E} &= E/E_0. \end{aligned} \quad (13)$$

In the same manner, we define dimensionless parameters and variables

$$\begin{aligned} \tilde{\gamma} &= \gamma t_0, & \tilde{a} &= aE_0^2, & \tilde{x} &= x/x_0, & \tilde{k} &= kx_0, & \tilde{\Lambda} &= \Lambda/x_0 = 1.76, \\ \tilde{\omega} &= \omega t_0, & \tilde{\omega}' &= \omega'/c, & \tilde{\omega}'' &= \omega''/(cx_0), & \tilde{t} &= t/t_0, \end{aligned} \quad (14)$$

where $\tilde{\omega}' = \partial\tilde{\omega}/\partial\tilde{k}$ is the group velocity of the pulse and $\tilde{\omega}''$ the group dispersion. We also introduce a coordinate system $[\hat{x} = \tilde{x} - \alpha\tilde{t}, \hat{t} = \tilde{t}]$ moving uniformly in *space* along the \mathbf{x} -axis at normalized velocity α , in order to keep the *forward* propagating pulse slowly moving in the computational spatial mesh. We will show in Appendix B that the speed of this moving reference frame can be adjusted in order to reduce the numerical phase velocity error. We then obtain in the group velocity frame the following set of equations

$$\begin{cases} \tilde{H}_{\hat{t}} = \alpha\tilde{H}_{\hat{x}} + \tilde{E}_{\hat{x}}, \\ \tilde{D}_{\hat{t}} = \alpha\tilde{D}_{\hat{x}} + \tilde{H}_{\hat{x}}, \\ \tilde{\Phi}_{\hat{t}} = \alpha\tilde{\Phi}_{\hat{x}} + \tilde{U}, \\ \tilde{U}_{\hat{t}} = \alpha\tilde{U}_{\hat{x}} - 2\tilde{\gamma}\tilde{U} - \tilde{\omega}_1^2\tilde{\Phi} + \tilde{\beta}_1\tilde{\omega}_1^2\tilde{E}, \\ \tilde{D} = \tilde{E} + \tilde{\Phi} + \tilde{a}|\tilde{E}|^2\tilde{E}. \end{cases} \quad (15)$$

Applying the reductive perturbation method of Taniuti et al. [8] to Maxwell's equations in the group velocity $[\hat{x}, \hat{t}]$ representation, leads to lowest order of a perturbation expansion parameter

$\epsilon = \Delta\omega/\omega_0$ to the nonlinear Schrödinger (NLS) equation governing the envelope soliton evolution (in the slowly varying envelope approximation) :

$$i\tilde{q}_t + \frac{1}{2\tilde{T}_D}\tilde{q}_{\hat{x}\hat{x}} + \frac{1}{\tilde{T}_{NL}}|\tilde{q}|^2q = \mathcal{O}(\epsilon^3), \quad (16)$$

where the characteristic second-order dispersion and nonlinear length scales are defined as [3]

$$\tilde{T}_D = \frac{1}{\tilde{\omega}''}, \quad \tilde{T}_{NL} = \frac{2\tilde{k}}{\tilde{\omega}^2\tilde{\omega}'\tilde{a}}. \quad (17)$$

The balance between both length scales,

$$\tilde{T}_{NL}/\tilde{T}_D = 1, \quad (18)$$

provides the appropriate value for the nonlinear parameter

$$\tilde{a} = \frac{2\tilde{k}\tilde{\omega}''}{\tilde{\omega}^2\tilde{\omega}'}. \quad (19)$$

The nonlinear Schrödinger equation (16) was solved exactly by Zakharov and Shabat [10] using the inverse scattering method. The balance equation (18) was shown in this context to generate any order N -soliton solution of period $\tilde{T}_S = (\pi/2)\tilde{T}_D$.

The linear dispersion relation associated to the set of equations (15) is readily obtained using the spatial Fourier expansion of $\tilde{q}(\hat{x})$,

$$\begin{aligned} \tilde{E}(\hat{x}, \hat{t}) &= 1/(2\pi) \int_{-\infty}^{\infty} q(\hat{k}) \exp [i(\hat{k}\hat{x} - \hat{\omega}\hat{t})] d\hat{k}, \\ &= \tilde{q}(\hat{x}) \exp [i(\hat{k}_0\hat{x} - \hat{\omega}_0\hat{t})] \end{aligned} \quad (20)$$

where $\hat{\omega} = \hat{\omega}(\hat{k})$, $\hat{\omega} = \tilde{\omega} - \alpha\tilde{k}$, $\hat{k} = \tilde{k}$ and is given in terms of the normalized frequency $\tilde{\omega}$ (relative to the rest frame $[\tilde{x}, \tilde{t}]$) by

$$\tilde{\omega}^4 + 2i\tilde{\gamma}\tilde{\omega}^3 - [\tilde{k}^2 + (1 + \tilde{\beta}_1)\tilde{\omega}_1^2] \tilde{\omega}^2 - 2i\tilde{\gamma}\tilde{k}^2\tilde{\omega} + \tilde{k}^2\tilde{\omega}_1^2 = 0, \quad (21)$$

whose solution for $\tilde{\gamma} = 0$ is readily obtained as

$$\begin{aligned} \tilde{\omega} &= (1/\sqrt{2}) \sqrt{A + \sqrt{B}}, \\ A &= \tilde{k}^2 + (1 + \tilde{\beta}_1) \tilde{\omega}_1^2, \\ B &= A^2 - 4\tilde{\omega}_1^2\tilde{k}^2. \end{aligned} \quad (22)$$

We can eliminate \tilde{D} from (15) and write

$$\left\{ \begin{array}{l} \tilde{H}_t = \alpha\tilde{H}_{\hat{x}} + \tilde{E}_{\hat{x}}, \\ \tilde{E}_t + \tilde{a} (|\tilde{E}|^2\tilde{E})_t = \alpha [\tilde{E}_{\hat{x}} + \tilde{a} (|\tilde{E}|^2\tilde{E})_{\hat{x}}] + \tilde{H}_{\hat{x}} - \tilde{U}, \\ \tilde{\Phi}_t = \alpha\tilde{\Phi}_{\hat{x}} + \tilde{U}, \\ \tilde{U}_t = \alpha\tilde{U}_{\hat{x}} - 2\tilde{\gamma}\tilde{U} - \tilde{\omega}_1^2\tilde{\Phi} + \tilde{\beta}_1\tilde{\omega}_1^2\tilde{E}, \end{array} \right. \quad (23)$$

After some lengthy but straightforward algebraic manipulations, the following conservation law is found :

$$\int_{-\infty}^{+\infty} \mathcal{S}_{\hat{x}} d\hat{x} = -\frac{\partial}{\partial \hat{t}} \mathcal{E} - \frac{4\tilde{\gamma}}{\beta_1 \tilde{\omega}_1^2} \int_{-\infty}^{+\infty} |\tilde{U}|^2 d\hat{x}, \quad (24)$$

where \mathcal{S} is the magnitude of the Poynting vector defining the energy density flow,

$$\mathcal{S} = -\frac{1}{2}(\tilde{E}\tilde{H}^* + \tilde{E}^*\tilde{H}), \quad (25)$$

and

$$\mathcal{E} = \int_{-\infty}^{+\infty} (|\tilde{E}|^2 + |\tilde{H}|^2 + \frac{3\tilde{a}}{2}|\tilde{E}|^4 + \frac{1}{\beta_1}|\tilde{\Phi}|^2 + \frac{1}{\beta_1 \tilde{\omega}_1^2}|\tilde{U}|^2) d\hat{x}. \quad (26)$$

Since $\int_{-\infty}^{+\infty} \mathcal{S}_{\hat{x}} d\hat{x} = 0$ (conservation of the energy flow), the energy is conserved if $\tilde{\gamma} = 0$. We also note the invariance of the conservation law (24) under the Galilean transformation $[\tilde{x}, \tilde{t}] \rightarrow [\hat{x}, \hat{t}]$.

3 The Numerical Scheme

We will now introduce a finite-difference approximation defined on a discrete time and space mesh for the system of partial differential equations (23) defined in the continuum. The important property, which we will be concerned in the derivation of the scheme is that it should reproduce discrete analogs of the continuous conserved quantities. The existence of discrete conservation laws is important for the global accuracy of the scheme [11, 12] and will be at the basis of the generalized stability analysis. From now on, for simplicity we drop the tilda symbol over all fields and variables, bearing in mind their dimensionless form and denote the mesh sizes by $\chi = \Delta\hat{x}$, $\tau = \Delta\hat{t}$. We start by introducing the following centered difference derivatives

$$\begin{aligned} D^1 X_j^n &= \frac{1}{2\chi} (X_{j+1}^n - X_{j-1}^n), \\ G^1 X_j^n &= \frac{1}{2\tau} (X_j^{n+1} - X_j^{n-1}), \end{aligned} \quad (27)$$

operating on a discrete variable X_j^n defined on the discrete domain

$$Q_\chi \times Q_\tau = \{(\hat{x}_j = j\chi, \hat{t}_n = n\tau) \mid 1 \leq j \leq N, 1 \leq n \leq N'\}. \quad (28)$$

The deviation between the discrete difference operators and the corresponding differential ones is readily obtained from their respective action on the Fourier modes $\exp[i(k\hat{x} - \hat{\omega}\hat{t})]$, giving

$$\begin{aligned} D^1 &= i \frac{\sin(k\chi)}{\chi}, \\ G^1 &= -i \frac{\sin(\hat{\omega}\tau)}{\tau}, \end{aligned} \quad (29)$$

and hence

$$\begin{aligned} D^1 &= \partial/\partial\hat{x} + \mathcal{O}(\chi^2), \\ G^1 &= \partial/\partial\hat{t} + \mathcal{O}(\tau^2). \end{aligned} \quad (30)$$

To construct the conservative numerical scheme, we use *time and space* centered difference derivatives. We then obtain the following *explicit* leap-frog scheme for the system (23) :

$$\left\{ \begin{array}{l} (1/2\tau)(H_j^{n+1} - H_j^{n-1}) = \alpha D^1 H_j^n + D^1 E_j^n, \\ (1/2\tau)(E_j^{n+1} - E_j^{n-1}) + (a/2\tau)|E_j^n|^2(E_j^{n+1} - E_j^{n-1}) = \alpha D^1 E_j^n + \\ \quad + \alpha a |E_j^n|^2 D^1 E_j^n + D^1 H_j^n - (1/2)(U_j^{n+1} + U_j^{n-1}), \\ (1/2\tau)(\Phi_j^{n+1} - \Phi_j^{n-1}) = \alpha D^1 \Phi_j^n + (1/2)(U_j^{n+1} + U_j^{n-1}), \\ (1/2\tau)(U_j^{n+1} - U_j^{n-1}) = \alpha D^1 U_j^n - \gamma(U_j^{n+1} + U_j^{n-1}) - (\omega_1^2/2)(\Phi_j^{n+1} + \Phi_j^{n-1}) + \\ \quad + (\beta_1 \omega_1^2/2)(E_j^{n+1} + E_j^{n-1}). \end{array} \right. \quad (31)$$

The relevant features to be checked for the choice of the particular difference scheme are (1) its consistency, (2) the existence of a discrete conserved energy, (3) its stability and (4) convergence. Formally, the requirement of consistency, i.e. in the limit of small time and space steps, the difference system becomes identical to the differential one, can be checked using the Taylor expansions (30) yielding

$$\begin{aligned} (1/2)(X_j^{n+1} + X_j^{n-1}) &= X(\hat{x}_j, \hat{t}_n) + \mathcal{O}(\tau^2), \\ |E_j^n|^2(1/2\tau)(E_j^{n+1} - E_j^{n-1}) &= G^1 \left[|E_j^n|^2 E_j^n \right] + \mathcal{O}(\tau^2), \\ &= \left(|E|^2 E \right)_{\hat{t}} + \mathcal{O}(\tau^2). \end{aligned} \quad (32)$$

To verify the existence of a discrete conservation law, we multiply each difference equation by $(\chi/2)(Z_j^{n+1} + Z_j^{n-1})^*$ with Z respectively equal to H, E, Φ, U . Summing over the spatial mesh parameter j and adding the complex conjugate equations leads to the desired discrete conservation law :

$$\frac{\mathcal{E}^{n+1} - \mathcal{E}^n}{\tau} = - \left(\frac{\gamma}{\beta_1 \omega_1^2} \right) \chi \sum_{j \in Q_x} \left| U_j^{n+1} + U_j^{n-1} \right|^2, \quad (33)$$

where the discrete energy is given by

$$\begin{aligned} \mathcal{E}^{n+1} &= \chi \sum_{j \in Q_x} \left\{ |E_j^{n+1}|^2 + |E_j^n|^2 + a |E_j^{n+1}|^2 |E_j^n|^2 + |H_j^{n+1}|^2 + |H_j^n|^2 \right\} + \\ &\quad + \chi \sum_{j \in Q_x} \left\{ \frac{1}{\beta_1} (|\Phi_j^{n+1}|^2 + |\Phi_j^n|^2) + \frac{1}{\beta_1 \omega_1^2} (|U_j^{n+1}|^2 + |U_j^n|^2) \right\}. \end{aligned} \quad (34)$$

In the next section we analyze in detail the nonlinear stability and convergence of the difference scheme (31).

4 Nonlinear Stability and Convergence

To address and analyze the problem of stability and convergence, we need a measure of the difference between two “states” of the physical system modeled [13]. Obviously, this measure

should have the properties of a norm. In the present case, we introduce the discrete L^2 -norm defined by

$$\|v^n\|^2 = \langle v^n, v^n \rangle = \chi \sum_{j \in Q_\chi} v_j^n v_j^{*n}. \quad (35)$$

We can easily show that the discrete difference operator D^1 introduced in eq. (27) satisfy

$$\langle D^1 v^n, w^n \rangle = -\langle v^n, D^1 w^n \rangle. \quad (36)$$

This result can be understood as being the discrete analog of the integration by parts in L^2 . Hence, we obtain the following lemma

LEMMA 1.

$$\begin{aligned} \operatorname{Re} \langle D^1 v^n, w^n \rangle + \operatorname{Re} \langle D^1 v^n, w^n \rangle &= 0, \\ \operatorname{Re} \langle D^1 v^n, v^n \rangle &= 0. \end{aligned} \quad (37)$$

We give also another lemma considered by Lees et al. [5, 6, 7] as the main tool to be used in the study of stability of the numerical scheme.

LEMMA 2.

Let $f(n)$, $g(n)$ be nonnegative mesh functions. If $C \geq 0$ and $g(n)$ is nondecreasing and

$$f(n) \leq g(n) + C\tau \sum_{l=0}^{n-1} f(l), \quad (38)$$

then for all n we have

$$f(n) \leq g(n) \exp(Cn\tau). \quad (39)$$

We can now start the stability analysis.

Let $h^n(x)$, $e^n(x)$, $\varphi^n(x)$ and $u^n(x)$ be the errors of the numerical solution $H^n(x)$, $E^n(x)$, $\Phi^n(x)$ and $U^n(x)$ of (31) respectively. The errors always satisfy

$$\frac{1}{2\tau}(h^{n+1} - h^{n-1}) = \alpha D^1 h^n + D^1 e^n + a^n, \quad (40)$$

$$\begin{aligned} \frac{1}{2\tau}(e^{n+1} - e^{n-1}) + \frac{a}{2\tau}|e^n|^2(e^{n+1} - e^{n-1}) &= \alpha D^1 e^n + \alpha a|e^n|^2 D^1 e^n + D^1 h^n \\ -\frac{1}{2}(u^{n+1} + u^{n-1}) + \frac{1}{2\tau}S^n + R^n, \end{aligned} \quad (41)$$

$$\frac{1}{2\tau}(\varphi^{n+1} - \varphi^{n-1}) = \alpha D^1 \varphi^n + \frac{1}{2}(u^{n+1} + u^{n-1}) + c^n, \quad (42)$$

$$\begin{aligned} \frac{1}{2\tau}(u^{n+1} - u^{n-1}) &= \alpha D^1 u^n - \gamma(u^{n+1} + u^{n-1}) - \frac{\omega_1^2}{2}(\varphi^{n+1} + \varphi^{n-1}) \\ &+ \frac{\beta_1 \omega_1^2}{2}(e^{n+1} + e^{n-1}) + d^n, \end{aligned} \quad (43)$$

where a^n, b^n, c^n and d^n are truncation errors of order $\mathcal{O}(\tau^2 + \chi^2)$, and

$$R^n = \alpha a \left[|E^n|^2 D^1 E^n - |E^n + e^n|^2 D^1 (E^n + e^n) \right], \quad (44)$$

$$S^n = a \left[(|E^n|^2 - |E^n + e^n|^2)(E^{n+1} - E^{n-1}) + (|e^n|^2 - |E^n + e^n|^2)(e^{n+1} - e^{n-1}) \right], \quad (45)$$

where the nonlinear terms R^n, S^n satisfy

$$\text{Re}\langle R^n, (e^{n+1} + e^{n-1}) \rangle = \mathcal{O}(\tau^2), \quad (46)$$

$$\|S^n\| \leq M_1 \|e^n\| + M_2 (\|e^{n+1}\| + \|e^{n-1}\|), \quad (47)$$

with M_1 and M_2 constants depending only on the initial data.

Multiplying eqs.(40)-(43) by $(1/2)(z^{n+1} + z^{n-1})^*$ with z resp. equal to h, e, φ, u , taking the inner product and using the identities of Lemma 1, we obtain the following set of equations for the nonlinear error terms

$$\begin{aligned} (1/2\tau)(\|h^{n+1}\|^2 - \|h^{n-1}\|^2) &= \text{Re}\langle D^1 e^n, (h^{n+1} + h^{n-1}) \rangle + \text{Re}\langle a^n, (h^{n+1} + h^{n-1}) \rangle, \\ (1/2\tau)(\|e^{n+1}\|^2 - \|e^{n-1}\|^2) + (a/2\tau)(\|e^{n+1}e^n\|^2 - \|e^n e^{n-1}\|^2) &= \text{Re}\langle D^1 h^n, (e^{n+1} + e^{n-1}) \rangle \\ &+ (1/2\tau)\text{Re}\langle S^n, (e^{n+1} + e^{n-1}) \rangle + \text{Re}\langle b^n, (e^{n+1} + e^{n-1}) \rangle - (1/2)\text{Re}\langle (u^{n+1} + u^{n-1}), (e^{n+1} + e^{n-1}) \rangle, \\ (1/2\tau)(\|\varphi^{n+1}\|^2 - \|\varphi^{n-1}\|^2) &= (1/2)\text{Re}\langle (u^{n+1} + u^{n-1}), (\varphi^{n+1} + \varphi^{n-1}) \rangle + \text{Re}\langle c^n, (\varphi^{n+1} + \varphi^{n-1}) \rangle, \\ (1/2\tau)(\|u^{n+1}\|^2 - \|u^{n-1}\|^2) &= -\frac{\omega_1^2}{2}\text{Re}\langle (u^{n+1} + u^{n-1}), (\varphi^{n+1} + \varphi^{n-1}) \rangle \\ &+ \frac{\beta\omega_1^2}{2}\text{Re}\langle (u^{n+1} + u^{n-1}), (e^{n+1} + e^{n-1}) \rangle - \gamma\|u^{n+1} + u^{n-1}\|^2 + \text{Re}\langle d^n, (u^{n+1} + u^{n-1}) \rangle. \end{aligned} \quad (48)$$

Combining all these equations, we obtain

$$\begin{aligned} \frac{1}{2\tau}(\|e^{n+1}\|^2 - \|e^{n-1}\|^2) + \frac{a}{2\tau}\|e^n\|^2(\|e^{n+1}\|^2 - \|e^{n-1}\|^2) + \frac{1}{2\beta_1\tau}(\|\varphi^{n+1}\|^2 - \|\varphi^{n-1}\|^2) \\ + \frac{1}{2\beta_1\omega_1^2\tau}(\|u^{n+1}\|^2 - \|u^{n-1}\|^2) = \\ \frac{1}{2\tau}\text{Re}\langle S^n, (e^{n+1} + e^{n-1}) \rangle + \text{Re}\langle D^1 h^n, (e^{n+1} + e^{n-1}) \rangle + \text{Re}\langle b^n, (e^{n+1} + e^{n-1}) \rangle \\ + \frac{1}{\beta_1}\text{Re}\langle c^n, (\varphi^{n+1} + \varphi^{n-1}) \rangle + \frac{1}{\beta_1\omega_1^2}\text{Re}\langle d^n, (u^{n+1} + u^{n-1}) \rangle - \frac{\gamma}{\beta_1\omega_1^2}\|u^{n+1} + u^{n-1}\|^2, \end{aligned} \quad (49)$$

which can be rewritten as

$$\begin{aligned}
& \frac{1}{2\tau}(\|h^{n+1}\|^2 - \|h^{n-1}\|^2) + \frac{1}{2\tau}(\|e^{n+1}\|^2 - \|e^{n-1}\|^2) + \frac{a}{2\tau}(\|e^{n+1}e^n\|^2 - \|e^n e^{n-1}\|^2) \\
& + \frac{1}{2\beta_1\tau}(\|\varphi^{n+1}\|^2 - \|\varphi^{n-1}\|^2) + \frac{1}{2\beta_1\omega_1^2\tau}(\|u^{n+1}\|^2 - \|u^{n-1}\|^2) = \\
& + \frac{1}{2\tau}Re\langle S^n, (e^{n+1} + e^{n-1}) \rangle + Re\langle a^n, (h^{n+1} + h^{n-1}) \rangle + Re\langle b^n, (e^{n+1} + e^{n-1}) \rangle \\
& + \frac{1}{\beta_1}Re\langle c^n, (\varphi^{n+1} + \varphi^{n-1}) \rangle + \frac{1}{\beta_1\omega_1^2}Re\langle d^n, (u^{n+1} + u^{n-1}) \rangle - \frac{\gamma}{\beta_1\omega_1^2}\|u^{n+1} + u^{n-1}\|^2.
\end{aligned} \tag{50}$$

Summing the above equality for $t = \tau, 2\tau, \dots, n\tau$ yields the following expression

$$\begin{aligned}
& \|(z^{n+1}, z^n)\|^2 + a\|e^{n+1}e^n\|^2 = \|(z^1, z^0)\|^2 + a\|e^1e^0\|^2 - \frac{2\tau\gamma}{\beta_1\omega_1^2} \sum_{m=1}^n \|u^{m+1} + u^{m-1}\|^2 \\
& + \sum_{m=1}^n Re\langle S^m, (e^{m+1} + e^{m-1}) \rangle + 2\tau \sum_{m=1}^n Re\langle a^m, (h^{m+1} + h^{m-1}) \rangle + 2\tau \sum_{m=1}^n Re\langle b^m, (e^{m+1} + e^{m-1}) \rangle \\
& + \frac{2\tau}{\beta_1} \sum_{m=1}^n Re\langle c^m, (\varphi^{m+1} + \varphi^{m-1}) \rangle + \frac{2\tau}{\beta_1\omega_1^2} \sum_{m=1}^n Re\langle d^m, (u^{m+1} + u^{m-1}) \rangle,
\end{aligned} \tag{51}$$

where

$$\begin{aligned}
\|(z^{n+1}, z^n)\|^2 & = \|h^{n+1}\|^2 + \|h^n\|^2 + \|h^{n+1}\|^2 + \|h^n\|^2 + \frac{1}{\beta_1}(\|\varphi^{n+1}\|^2 + \|\varphi^n\|^2) \\
& + \frac{1}{\beta_1\omega_1^2}(\|u^{n+1}\|^2 + \|u^n\|^2).
\end{aligned} \tag{52}$$

Applying the triangular inequality $Re\langle v, w \rangle \leq (1/2)(\|v\|^2 + \|w\|^2)$ to each real part term in the previous equation yields

$$\begin{aligned}
\|(z^{n+1}, z^n)\|^2 & \leq \|(z^1, z^0)\|^2 + a\|e^1e^0\|^2 + \left(\frac{1}{2} + \tau\right) \sum_{m=1}^n \|e^{m+1} + e^{m-1}\|^2 + \tau \sum_{m=1}^n \|h^{m+1} + h^{m-1}\|^2 \\
& + \frac{\tau}{\beta_1} \sum_{m=1}^n \|\varphi^{m+1} + \varphi^{m-1}\|^2 + \frac{\tau(1-2\gamma)}{\beta_1\omega_1^2} \sum_{m=1}^n \|u^{m+1} + u^{m-1}\|^2 + \tau \sum_{m=1}^n \|f^m\|^2 + \frac{1}{2} \sum_{m=1}^n \|S^m\|^2,
\end{aligned} \tag{53}$$

where

$$\|f^m\|^2 = \|a^m\|^2 + \|b^m\|^2 + \frac{1}{\beta_1}\|c^m\|^2 + \frac{1}{\beta_1\omega_1^2}\|d^m\|^2. \tag{54}$$

Using the inequality (47) for the norm of the nonlinear term $\|S^m\|$, transforms (53) into

$$\begin{aligned}
\|(z^{n+1}, z^n)\|^2 & \leq \|(z^1, z^0)\|^2 + a\|e^1e^0\|^2 + C_0\tau \sum_{m=0}^n (\|e^{m+1}\|^2 + \|e^m\|^2) + 2\tau \sum_{m=0}^n (\|h^{m+1}\|^2 + \|h^m\|^2) \\
& + \frac{\tau}{\beta_1} \sum_{m=0}^n (\|\varphi^{m+1}\|^2 + \|\varphi^m\|^2) + \frac{2\tau(1-2\gamma)}{\beta_1\omega_1^2} \sum_{m=0}^n (\|u^{m+1}\|^2 + \|u^m\|^2) + \tau \sum_{m=1}^n \|f^m\|^2,
\end{aligned} \tag{55}$$

which becomes using (52)

$$\|(z^{n+1}, z^n)\|^2 \leq \|(z^1, z^0)\|^2 + a\|e^1 e^0\|^2 + \tau \sum_{m=1}^n \|f^m\|^2 + C\tau \sum_{m=1}^{n+1} \|(z^m, z^{m-1})\|^2, \quad (56)$$

where C is a constant depending on the initial data only. Applying Lemma 1, we finally arrive at the desired energy norm inequality expressed by the following Theorem :

THEOREM 1.

Let τ be suitably small such that $1 - C\tau > 0$, then

$$\|(z^{n+1}, z^n)\|^2 \leq \frac{1}{K} \left(\|(z^1, z^0)\|^2 + a\|e^1 e^0\|^2 + \tau \sum_{m=1}^n \|f^m\|^2 \right) \exp\left(\frac{C(n+1)}{K}\right), \quad (57)$$

where C and K being positive constants depending only on the initial data. This theorem expresses the generalized stability of the numerical scheme (31) in the sense studied by Guo Ben-Yu [6].

We now consider the convergence of the scheme. We denote by \bar{H} , \bar{E} , $\bar{\Phi}$ and \bar{U} continuous, differentiable functions solution of the differential system (23), and by $H^n(x)$, $E^n(x)$, $\Phi^n(x)$, $U^n(x)$, the numerical solution of the difference system (31). For a discussion of convergence, we need a measure of the difference between the exact and the computed solution. We denote this error by $\bar{h}^n(x)$, $\bar{e}^n(x)$, $\bar{\varphi}^n(x)$, $\bar{u}^n(x)$ for x belonging to the discrete lattice Q_χ . The discussion then follows the same spirit as for the stability. The numerical errors satisfy formally a set of equations like (40)-(43). Applying the results of Theorem 1, we obtain an equivalent inequality for the numerical errors, expressed by the following Theorem :

THEOREM 2.

If τ is suitably small such that $1 - \bar{C}\tau = \bar{K} > 0$ then,

$$\|(\bar{z}^{n+1}, \bar{z}^n)\|^2 \leq \frac{1}{\bar{K}} \left(\|(\bar{z}^1, \bar{z}^0)\|^2 + a\|\bar{e}^1 \bar{e}^0\|^2 + \tau \sum_{m=1}^n \|\bar{f}^m\|^2 \right) \exp\left(\frac{\bar{C}(n+1)}{\bar{K}}\right), \quad (58)$$

where \bar{C} , \bar{K} are positive constants depending only on the initial data. This theorem means that the numerical errors are bounded by the initial and truncation errors, so the scheme is convergent.

5 Numerical Results

In this section we present results of the numerical simulations performed to test the stability and global accuracy of the conservative finite difference scheme (31). For clarity we rewrite the tilda symbols over all fields and variables to recall their dimensionless form. We have a completely explicit 3-level, 5-points scheme with four unknowns \tilde{H}_j^{n+1} , \tilde{E}_j^{n+1} , $\tilde{\Phi}_j^{n+1}$, \tilde{U}_j^{n+1} at each

time level $n + 1$. The scheme is therefore not self-starting and a boot-strapping method is used to compute the fields at the first time level $n = 1$ from the initial data at $n = 0$. Specifically, the boot-strapping technique first advances the numerical solution from $\hat{t} = 0$ to $\hat{t} = \tau/8$ using the difference equations (31) with field values such as \tilde{E}_j^{n-1} for $n = 0$ replaced by $(\tilde{E}_{j-1}^0 + \tilde{E}_{j+1}^0)/2$ etc. Our scheme is then used to advance the solution successively from $\hat{t} = \tau/8$ to $\tau/4$, $\tau/2$, τ . Approximate initial conditions $\tilde{Z}(\hat{x}, \hat{t} = 0)$ can be obtained using the Fourier transform solution of the linear part of the differential system (23). Choosing the initial electric field of the form (20) with $\tilde{q}(\hat{x}) = \eta_1 \text{sech}(\hat{x})$ and assuming that the Fourier amplitudes

$$Z(\tilde{k}) = \int \tilde{Z}(\hat{x}, \hat{t} = 0) \exp(-i\tilde{k}\hat{x}) d\hat{x},$$

with $Z = H, \Phi$ or U , have a narrow bandwidth around $\tilde{k} = \tilde{k}_0$, we can expand them in a Taylor series, yielding

$$\tilde{Z}(\hat{x}, \hat{t} = 0) = \left[Z(\tilde{k}_0)\tilde{q}(\hat{x}) - iZ_{\tilde{k}}(\tilde{k}_0)\tilde{q}_{\hat{x}}(\hat{x}) - (1/2)Z_{\tilde{k}\tilde{k}}(\tilde{k}_0)\tilde{q}_{\hat{x}\hat{x}}(\hat{x}) + \dots \right] \exp(i\tilde{k}_0\hat{x}). \quad (59)$$

The boundary conditions implemented to solve the difference system (31) are absorbing boundary conditions minimizing reflections at the end points of the mesh. Since we are interested in solitonlike solutions, the presence of linear dispersive radiation is expected to be small and we can therefore use simple linear dispersionless boundary conditions obtained by setting $\tilde{a}, \tilde{\Phi}$ and \tilde{U} equal to zero in the differential equations (23). Allowing only for outgoing waves at the boundaries corresponds to prescribe $\tilde{E} = -\tilde{H}$ at the right-hand boundary and $\tilde{E} = \tilde{H}$ at the left-hand boundary.

We take the value of the initial hyperbolic secant pulse characteristic time constant t_0 equal to $14.6 \cdot 10^{-15} \text{s}$, ($x_0 = 4.38 \mu\text{m}$), the medium resonance frequency and strength $\tilde{\omega}_1 = 6$, $\beta_1 = 3$, as in the work of Hile and Kath [4], and use a small value of damping rate $\tilde{\gamma} = 10^{-9}$. We are currently investigating a new conservative finite-difference time domain scheme to model the finite response time of the nonlinear susceptibility $\chi^{(3)}$ (the Raman effect) in (3), which becomes important for optical femtosecond pulses. The advantage of modeling directly Maxwell's equations instead of nonlinear Schrödinger type equations for slowly varying envelopes is that in the present approach the modeling of the optical carrier $\exp(i\tilde{k}_0\hat{x})$ is retained. We choose the carrier wavelength $\tilde{\lambda}_0 = 2\pi/\tilde{k}_0$ equal to $(1/4)\tilde{\Lambda}$ and $(1/8)\tilde{\Lambda}$ where $\tilde{\Lambda}$ (FWHM) is equal to 1.76. The corresponding values of frequency, group velocity and group velocity dispersion are obtained from the linear dispersion relation (22). The appropriate value for the nonlinear parameter \tilde{a} is found from (19). Finally, by choosing a uniform spatial resolution of 100 steps per carrier wavelength, $\chi = \tilde{\lambda}_0/100 = 44 \cdot 10^{-4}$, [$\tilde{\lambda}_0 = (1/4)\tilde{\Lambda}$] and adjusting the value of α to the group velocity ω' plus a small correction (a temporal resolution $\tau = (1/2)\chi$ obtained from (A3) is suitable), we can reduce the numerical phase velocity error to 10^{-5} as shown in Appendix B.

In Fig. (1) we present the electric field profiles at the initial time, after half and two soliton periods, for the case of a fixed initial pulse width (FWHM equals to $\Lambda = 1.76 x_0 = 7.71 \mu\text{m}$ containing 8 and 4 optical carrier wavelengths. For the 8 cycle case ($\tilde{\lambda}_0 = \tilde{\Lambda}/8$), soliton parameters are given by $\tilde{\omega}_0 = 30.46$, $\tilde{\omega}' = 0.93$, $\tilde{\omega}'' = 0.0047$, $\tilde{a} = 0.0003$, $\tilde{T}_S \sim 336$, while for the 4 cycle case ($\tilde{\lambda}_0 = \tilde{\Lambda}/4$), they are $\tilde{\omega}_0 = 18$, $\tilde{\omega}' = 0.76$, $\tilde{\omega}'' = 0.028$, $\tilde{a} = 0.0032$, $\tilde{T}_S \sim 57$. It is clear from these plots that the solitons are stable pulse solutions for a wide range of parameter values. In both cases, the appearance of an asymmetry in the leading edge of the pulse as a

consequence of the higher-order dispersion is noticeable. The results in Fig. (2) display the maximum electric field magnitude for initial 3-, 2- and fundamental soliton pulses. We observe an interesting wavelength-dependent effect, namely the shift of the amplitude peak to later times for larger wavelengths (look at the dashed lines corresponding to the 4 cycle pulse). We provide the energy plots in Fig. (3). As in the previous figure, a temporal oscillatory pattern for higher-order solitons is observable. The tiny oscillations of the energy, appear presumably as a result of the nonsoliton part of the initial pulses. Finally, the numerical phase velocity error as given by (B4) is computed in Fig. (4). The cross on both graphs indicates the value of the numerical phase error at the group velocity $\alpha = \tilde{\omega}'$. Simulations have been carried out with α chosen to reduce the error to 10^{-5} .

6 Conclusions

In this paper we have presented numerical results for Maxwell's equations describing soliton propagation in nonlinear dispersive media reported in [4]. We proposed a particular conservative finite-difference scheme to solve the coupled differential equations based on the existence of a discrete conservation law corresponding to the underlying continuous energy conservation law. We proved that this property provides the stability and global accuracy of the algorithm. In the numerical simulations, initial hyperbolic secant pulse shapes of fixed full width at half peak intensity $\Lambda = 7.71\mu m$, containing as few as 4 and 8 optical carrier wavelengths were considered. We computed the temporal evolution of the pulse profile, the maximum field amplitude, and the energy for initial fundamental, second and third-order solitons. Further extension of this method to the case of a finite response time of the nonlinearity is under current investigation.

Acknowledgements

L.Gilles is grateful to the Ministerio de Educación y Cultura of Spain for a postdoctoral research grant. L.Vázquez thanks partial support from the Comisión Interministerial de Ciencia y Tecnología of Spain (PB95-0426).

Appendix A : Linear stability

We consider the stability of the linear part of the first-order partial differential equations (23), which can be cast in the form of a symmetric Friedrichs system [9] :

$$Z_{\hat{t}} + \mathcal{A}Z_{\hat{x}} + \mathcal{A}_0Z = 0, \quad (\text{A1})$$

where $Z = [H, E, \Phi, U]^T$ and

$$\mathcal{A} = \begin{bmatrix} -\alpha & -1 & 0 & 0 \\ -1 & -\alpha & 0 & 0 \\ 0 & 0 & -\alpha & 0 \\ 0 & 0 & 0 & -\alpha \end{bmatrix}, \quad \mathcal{A}_0 = \begin{bmatrix} 0 & 0 & 0 & 0 \\ 0 & 0 & 0 & -1 \\ 0 & 0 & 0 & 1 \\ 0 & \beta_1\omega_1^2 & -\omega_1^2 & -2\gamma \end{bmatrix}. \quad (\text{A2})$$

Since \mathcal{A} is symmetric and \mathcal{A}_0 constant, we have a Friedrichs system. We can then apply the general stability results for finite-difference schemes approaching (A2). In particular for the leap-frog method (5 points-three levels) we have the stability condition $\rho(\mathcal{A})\tau/\chi < 1$ where $\rho(\mathcal{A})$ is the spectral range of \mathcal{A} and is equal in the present case to $1 + \alpha$. We therefore obtain the following stability condition for the leap-frog method :

$$\frac{\tau}{\chi} < \frac{1}{1 + \alpha}. \quad (\text{A3})$$

We expect this upper mesh size ratio to be valid also for the nonlinear conservative scheme if the nonlinearity is sufficiently weak (i.e. for sufficiently small optical carrier wavelengths). Finally, note that if Φ is equal to zero, the finite-difference scheme is consistent with the underlying continuous duality property of Maxwell's equations.

Appendix B : Numerical Dispersion

To calculate the numerical dispersion, we substitute the Fourier components $\tilde{Z}_j^n = Z \exp[ikj\chi - \hat{\omega}_{num}\tau]$ with $Z = H, E, \Phi, U$ into the difference scheme (31), neglecting the nonlinear and damping constants $\tilde{a}, \tilde{\gamma}$. The following dispersion relation relative to the rest frame $[\tilde{x}, \tilde{t}]$ is then found :

$$\tilde{\omega}_{num}^4 - \tilde{\omega}_{num}^2 \left[\frac{\sin^2(k\chi)}{\chi^2} + \tilde{\Omega}_1^2(1 + \tilde{\beta}_1) \right] \tilde{\Omega}_1^2 \frac{\sin^2(k\chi)}{\chi^2} = 0, \quad (\text{B1})$$

where

$$\tilde{\Omega}_1^2 = \tilde{\omega}_1^2 \cos^2(\hat{\omega}_{num}\tau), \quad (\text{B2})$$

and

$$\tilde{\omega}_{num} = \frac{\sin(\hat{\omega}_{num}\tau)}{\tau} + \alpha \frac{\sin(k\chi)}{\chi}. \quad (\text{B3})$$

The solution of (B1, B2) provides the value for the numerical dispersion $\hat{\omega}_{num}$ relative to the moving frame. The error in the phase of the pulse can then be computed as

$$\epsilon(\alpha) = \frac{|\hat{\omega}_{num} - \hat{\omega}|}{\hat{\omega}}, \quad (\text{B4})$$

where $\hat{\omega} = \tilde{\omega} - \alpha k$ is obtained from (22).

References

- [1] A.Taflove, Wave Motion **10**, 547 (1988) and references therein.
- [2] P.M.Goorjian, A.Taflove, R.M.Joseph and S.C.Hagness, IEEE J.Quant.Electron. **28**, 2416 (1992); P.M.Goorjian and A.Taflove, Opt.Lett. **17**, 180 (1992).
- [3] G.P.Agrawal, “*Nonlinear Fiber Optics*”, Academic Press (1995).
- [4] C.V.Hile and W.L.Kath, J.Opt.Soc.Am.B **13**, 1135 (1996).
- [5] M.Lees, Trans.Amer.Math.Soc. **94**, 58 (1960);
- [6] Guo Ben-Yu, Appl.Math.Comp. **18**, 1 (1986); Z. Fei and L. Vázquez, Appl.Math.Comput. **45**, 17 (1991).
- [7] Guo Ben-Yu, I.Martín, V.M.Pérez García and L.Vázquez, J.Comp.Phys. **129**, 181 (1996).
- [8] T.Taniuti, “*Reductive perturbation method and far fields of wave equations*”, Prog. Theor. Phys. (Japan), suppl. **55**, 1 (1974).
- [9] R.Dautray and J-L.Lions “*Analyse mathématique et calcul numérique pour les sciences et les techniques*”, Vol. **9**, Masson (1988).
- [10] V.E.Zakharov and A.B.Shabat, Sov.Phys. JETP **34**, 62 (1972).
- [11] D.Potter, “*Computational Physics*”, Wiley (1973).
- [12] V. Konotop and L. Vázquez, “*Nonlinear Random Waves*”, World Scientific (1994).
- [13] P.D.Lax and R.D.Richtmyer, Comm.Pure Appl. Math. **IX**, 267 (1956).

Figure captions

Figure 1. Electric field pulse profiles at the initial time (dashed lines), after half and two soliton periods. Left plots refer to the case of an optical carrier wavelength equal to $\tilde{\lambda}_0 = \tilde{\Lambda}/8$ where $\tilde{\Lambda} = 1.76$ is the full width at half peak intensity (FWHM). Right plots are for $\tilde{\lambda}_0 = \tilde{\Lambda}/4$. Initial fundamental, 2- and 3-soliton pulses are considered.

Figure 2. Maximum electric field magnitude for initial soliton parameters as in the previous figure. The dashed line is for the large wavelength case $\tilde{\lambda}_0 = \tilde{\Lambda}/4$.

Figure 3. Electromagnetic energy as given by (34) for initial fundamental, 2- and 3-soliton pulses containing 8 or 4 optical carrier wavelengths.

Figure 4. Numerical phase error as given by (B4).

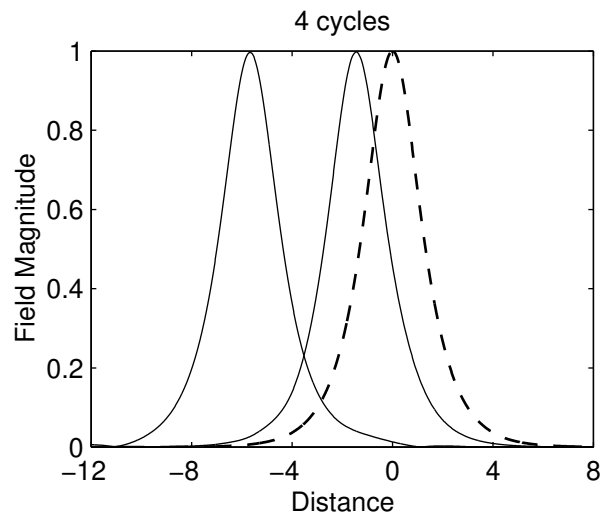
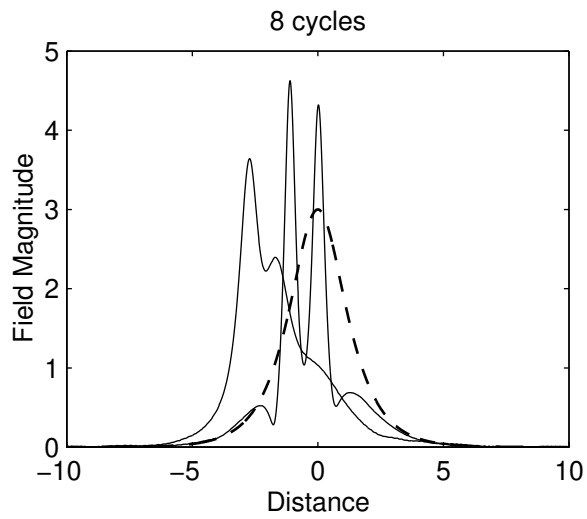
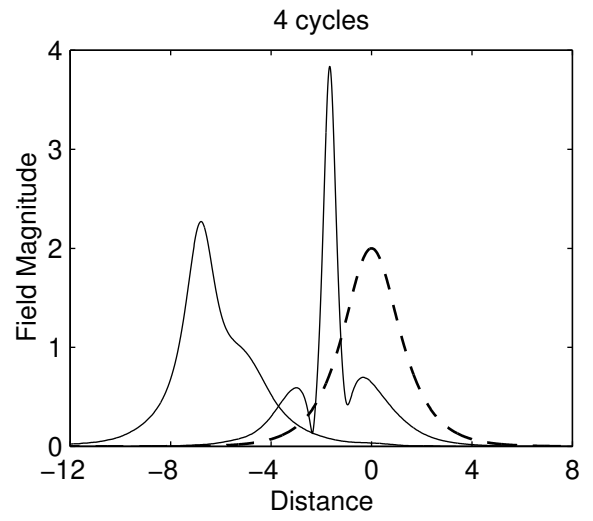
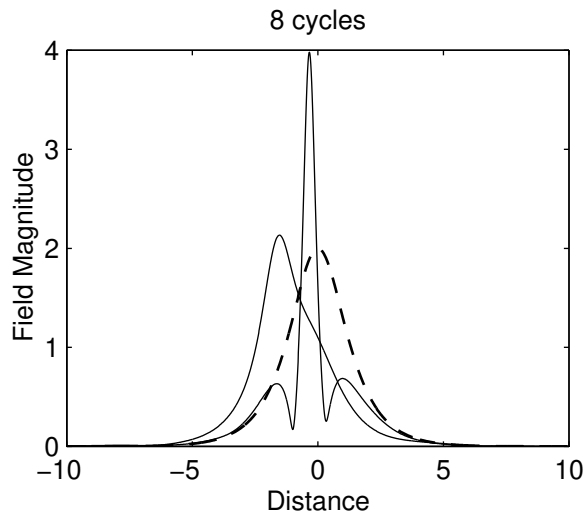


Fig.1

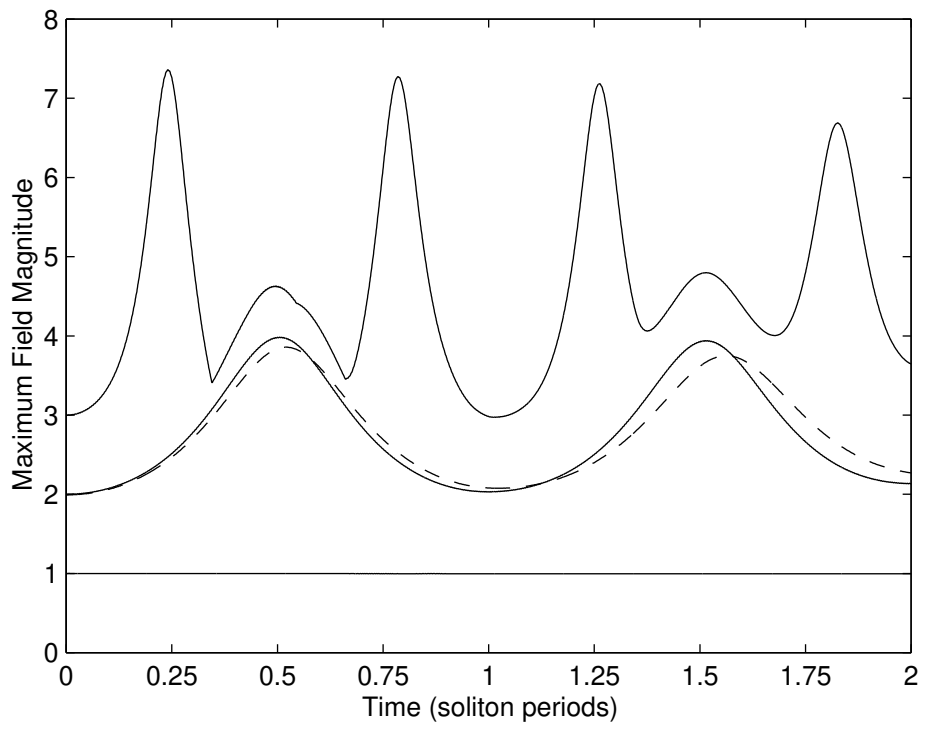


Fig.2

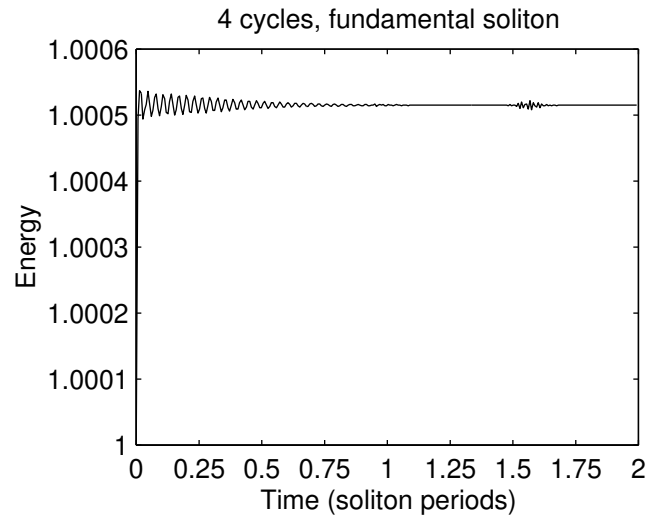
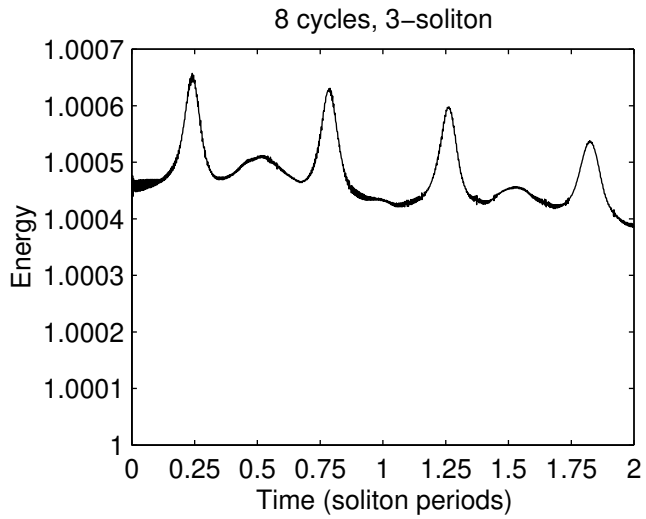
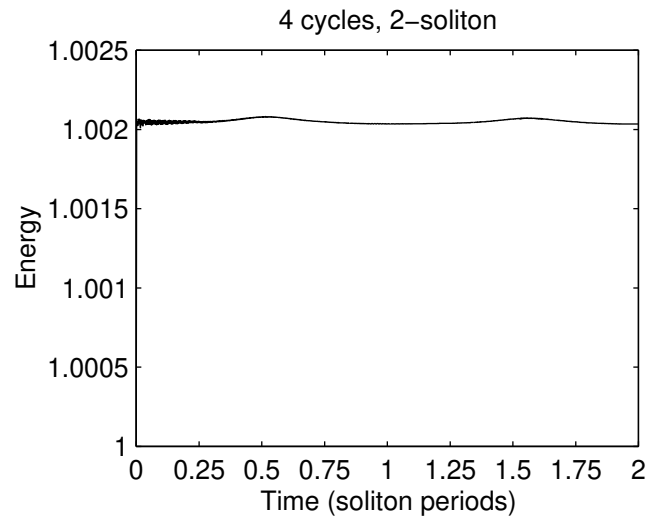
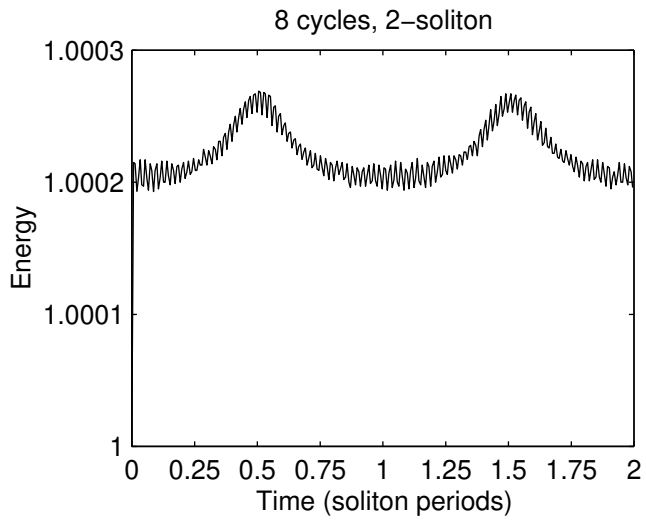


Fig.3

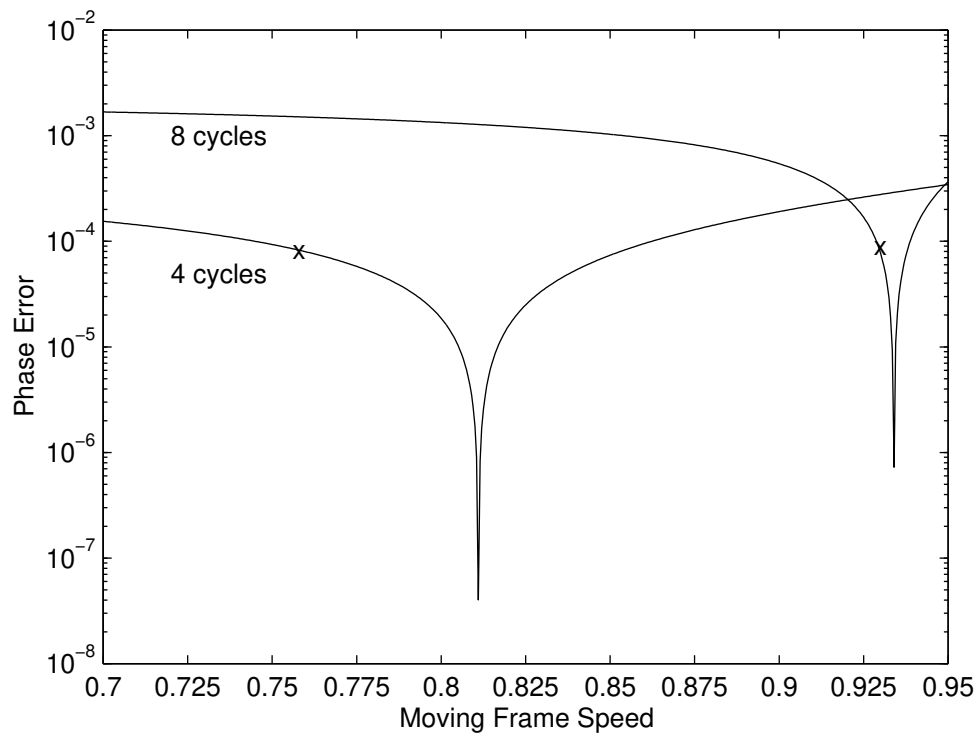


Fig.4